

Fully Unsupervised M-FISH Chromosome Image Characterization

Petros S. Karvelis and Aristidis C. Likas, *Senior Member, IEEE*

Abstract—Chromosome analysis is an important and difficult task for clinical diagnosis and biological research. A color imaging technique, multiplex fluorescent *in situ* hybridization (M-FISH), has been developed to ease the analysis of the process. Using an M-FISH technique each chromosome class (1,2, . . . ,22,X,Y) is stained with a unique color. However, significant variations between images are observed due to a number of factors such as uneven hybridization and spectral overlap among channels. These types of variations influence the pixel classification accuracy of image classification methods which are supervised and require a set of annotated images for training. In this paper, we present a fully unsupervised M-FISH chromosome image classification methodology. Our main contributions are 1) the assumption that the intensity of a chromosome pixel is sampled from multiple Gaussian components [Gaussian mixture model (GMM)] such that each component corresponds to one chromosome class, and 2) the initialization of the GMM model using the emission information of each chromosome class. This is feasible since prior to the M-FISH image acquirement, we already know which chromosome class is emitting to each of the five M-FISH image channels. The method has been tested on a large number of M-FISH images and an overall accuracy of 89.85% is reported. Our method is unsupervised and presents higher classification accuracy even when it is compared with common supervised based methods. Since the developed classification method does not require training data, it is highly convenient when ground truth does not exist.

Index Terms—Chromosomes, expectation-maximization (EM), multiplex fluorescent *in situ* hybridization (M-FISH), MAP-EM.

I. INTRODUCTION

CHROMOSOMES are the genetic information carriers of the DNA. For a normal human being, the number of chromosomes in a cell is 46, which consist of 22 pairs of similar, homologous chromosomes and two sex determinative chromosomes (XY: male, XX: female) [1]. The latest frontier is cancer cytogenetics analyzing chromosomal aberrations in malignant tissues [2]. The main obstacle to the wide implementation of cytogenetics prenatal screening and other diagnostic procedures [3] is that karyotyping, the procedure of chromosome classification, is very time consuming and it demands high quality of human resources. To ease the procedure of chromosome classification for the cytogeneticists, a color chromosome painting technique has been proposed in the mid-90s [4], [5].

Manuscript received October 10, 2012; revised March 9, 2013; accepted April 11, 2013. Date of publication April 24, 2013; date of current version November 12, 2013.

The authors are with the Department of Computer Science, University of Ioannina, GR 45110 Ioannina, Greece (e-mail: pkarvel@cs.uoi.gr; arly@cs.uoi.gr).

Color versions of one or more of the figures in this paper are available online at <http://ieeexplore.ieee.org>.

Digital Object Identifier 10.1109/JBHI.2013.2258931

This technique, which is called multiplex fluorescent *in situ* hybridization (M-FISH), uses five color dyes that attach to specific sequences of DNA in a way that each chromosome class absorbs a unique combination of dyes. Also, a sixth dye which is called DAPI is used to counterstain the chromosomes.

A fluorescent microscope with multiple optical filters is used to capture an M-FISH image, where each of the dyes is visible in one of the spectral channels. Using combinatorial labeling for an ideal M-FISH image, it is easy to determine the most likely chromosomal origin for each pixel as each fluor is either present—1—or absent—0— [6]. Several sets of fluors (kits) have been proposed for each chromosome class using three different color kits (Appendix A: Kit-A, Kit-B, and Kit-C).

M-FISH imaging has been widely used to detect chromosome anomalies. A common type of anomaly that is detected in cancer cells is translocations [7]. Translocation is a chromosome anomaly where exchange of chromosome material between the same or different chromosome classes takes place. This type of chromosome anomaly is very common in cancerous cells, and M-FISH imaging greatly simplifies the detection of such chromosome translocations since a chromosome now is displayed with two colors [8]. Fig. 1 presents two examples of translocations between two different classes of chromosomes.

Although the M-FISH imaging ease the process of karyotyping [3], [4], visual inspection of these images is a laborious and time-consuming process. Also the characterization of chromosome anomalies is difficult, since small rearrangements of chromosome material are difficult to identify for untrained personnel. For this reason, many attempts have been made to automate the whole or part of the classification of M-FISH images process [9]–[22].

The methods described in the literature either first segment the image and then classify the pixels of the image [12], [15], [17]–[21] or they directly classify all the pixels of the M-FISH image including a class for the background [11], [13], [14], [16]. In addition, these methods can be divided into following two categories based on the use of annotated images as a training set.

- 1) *Supervised* [11], [13]–[17], [20]: In a typical supervised classification scheme, the goal is to train a classifier that can be used to predict previously unseen images. These methods require the existence of a number of annotated images to train a classifier (e.g., Bayes [11]).
- 2) *Unsupervised* [18], [19], [21]: These methods do not use a set of annotated M-FISH images to train the classifier. Although unsupervised classification methods have been proposed, they have been tested only to a small number of M-FISH images and they present low classification accuracy.

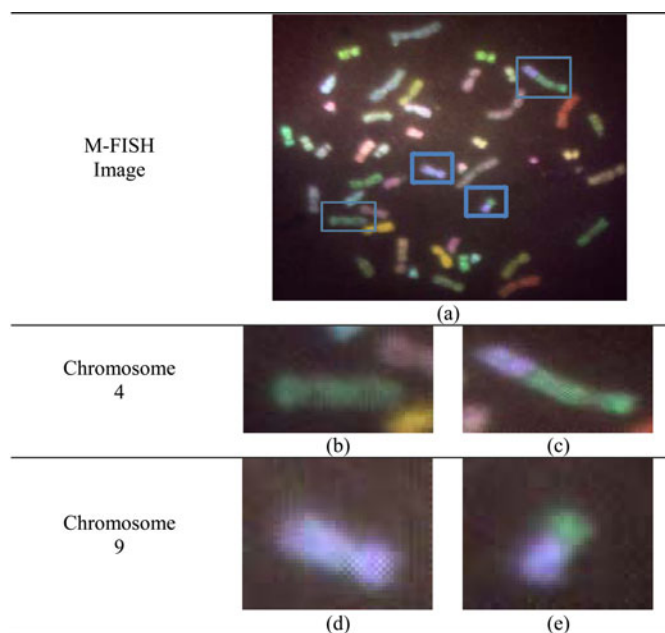
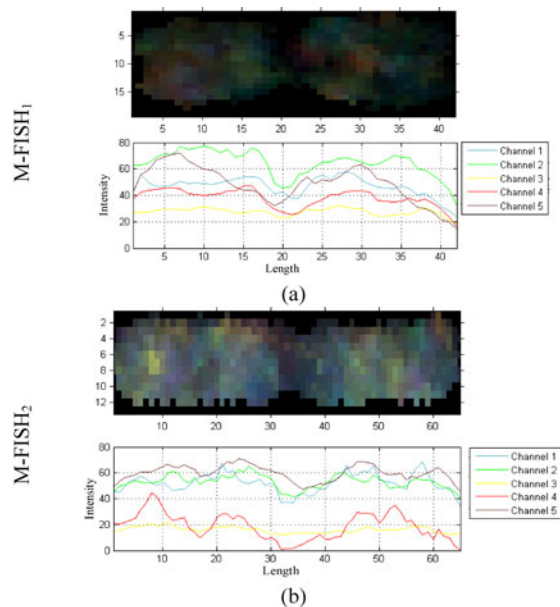


Fig. 1. M-FISH image with two translocations. Translocations between the chromosomes classes 4 and 9. (b) Normal chromosome of class 4 appearing with green color. (c) Abnormal chromosome of class 4 with translocation of class 9 appearing with different colors. (d) Normal chromosome of class 9 appearing with blue color. (e) Second homologue of chromosome class 9 with translocation of class 4 appearing with different colors.

One of the key factors limiting the supervised pixel classification accuracy is the variations between M-FISH images. This is due to the fact that the M-FISH imaging technique is not always accomplished under the same conditions, e.g., humidity, temperature, type of microscope, and color spread [21], [23] and these factors affect the quality of the produced M-FISH image. According to the color map of Kit-A, chromosome 3 should be ideally observed only in channels 1, 2, 4, and 5 and should not be visible in other channels.

Fig. 2 presents the color spread for two chromosomes of class 3 on two different M-FISH images (M-FISH₁, M-FISH₂). As one can observe, the chromosome in Fig. 2(a) presents a distribution of the fluor signal along the chromosome as the distribution described in the pattern of chromosome 3 [see Fig. 2(c)]. However, Fig. 2(b) presents the chromosome 3 for a different M-FISH image, where it is obvious that this chromosome has failed to hybridize on channel 4 [21]. Specifically, the average fluor for chromosome 3 of the channel 4 has a similar distribution such as the one the channel 3 [see Fig. 2(b)]. We can conclude that when the variation of the feature distribution across images is significant, which means the feature distribution of an unknown image is unpredictable, classification methods that rely on the estimation of class parameters (supervised methods) will yield low classification accuracy [21].

In this study, we propose an unsupervised method for the classification of M-FISH images. Unsupervised methods play an important role in many applications where the class labels are unavailable without requiring human visual comparisons or comparison with a preprocessed annotated image. Although these methods (e.g., Fuzzy C-Means [18]) have been already



Chromosome 3		Mean Value of Intensity for Chromosome 3	
Channel	Theoretic Pattern	M-FISH ₁	M-FISH ₂
1	1	51.8	58.4
2	1	62.3	57.8
3	0	27.2	18.6
4	1	39.8	20.3
5	1	47.9	59.5

(c)

Fig. 2. Two chromosomes of class 3 of two different M-FISH images (M-FISH₁, M-FISH₂). (a) Chromosome class 3 and its graph of average fluor signal along the chromosome of M-FISH₁. (b) Chromosome class 4 and its graph of average fluor signal along the chromosome of M-FISH₂. (c) Theoretic emission for each of the channels of chromosome class 3 and the mean value of intensity for chromosome 3 for the M-FISH images M-FISH₁ and M-FISH₂.

employed for the classification of M-FISH images, they have been applied only to a small number of M-FISH images failing to present a fully and robust unsupervised approach.

The main contribution of this study is the proposal of a new fully unsupervised classification method for the M-FISH images. Our unsupervised scheme is based on a multichannel Gaussian mixture model (GMM) with 24 components, one for each chromosome class. In order to overcome the problem of the initialization of the parameters of each GMM component, the first choice would be to randomly select parameter values or perform an initial clustering of the dataset. However, this would not incorporate the emission information of each chromosome class that we *a priori* had. In our case, the initialization is based on estimating the parameters of a single GMM via the expectation-maximization (EM) algorithm. Combining the parameters of the single-channel GMMs and the emission information of each chromosome class, an effective initial estimation of the multichannel GMM can be derived.

Although this initial GMM could accurately describe the chromosome distribution for an M-FISH image with high signal-to-noise ratio (SNR), this does not hold for images of low SNR.

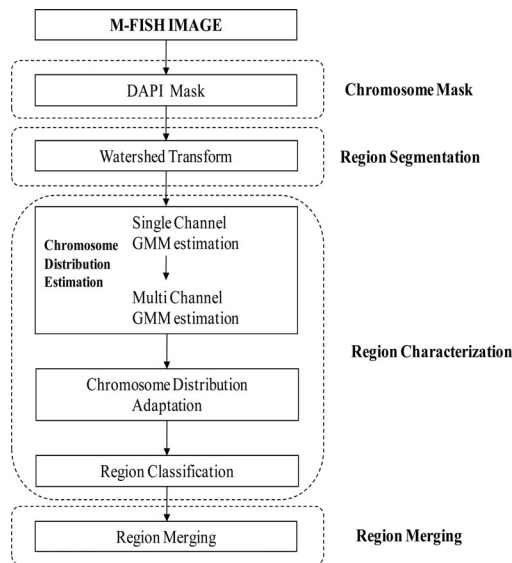


Fig. 3. Flowchart of the proposed method.

Thus, a further adaptation of the parameters of the multichannel GMM is needed. One straightforward approach is to use the classical EM algorithm starting from the initial estimation computed in the previous step. However, the large number of chromosome classes and the emission overlap could affect the mapping between each mixture component and each chromosome class. To overcome this problem, some kind of constraints should be applied on the GMM parameters. These constraints are naturally imported in the maximum *a-posteriori*-EM (MAP-EM) algorithm, which was used in our method. The estimation of the parameters using the MAP-EM method proves to be more effective in terms of classification accuracy over the classical EM algorithm. Furthermore, apart from effectively using the GMMs, the proposed method uses the watershed transform (WT) in order to segment the M-FISH image into regions (see Fig. 3). It has been already shown [20] that by classifying regions instead of pixels, a significant increase in the classification accuracy is obtained. Finally, the proposed method presents high classification accuracy, without any user interaction, even when compared with reported results using supervised classification methods.

The rest of the paper is organized as follows: In Section II, we provide all the details of the proposed method for unsupervised M-FISH image classification which is decomposed into following four different stages: 1) chromosome mask segmentation, where we compute an initial mask of the pixels to be classified, 2) the region segmentation stage, where the M-FISH image is decomposed into regions, 3) region classification, where the estimation of the parameters of the multichannel GMM takes places as well as the classification of each region, and finally, 4) region merging, where a final classification map is provided to the cytogeneticist. In Section III, we present numerical experiments that test the proposed method using the M-FISH image database [16]. Finally, we present discussion and conclusions in Section IV.

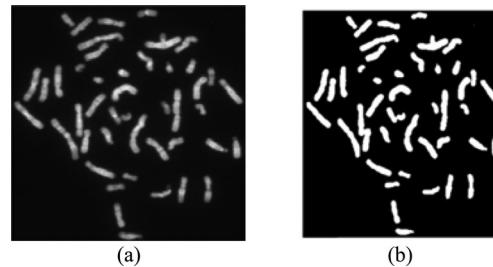


Fig. 4. Segmentation mask of a DAPI image. (a) DAPI image and (b) Segmentation mask $B_{Otsu}(i, j)$.

II. METHOD

Our method consists of four different stages (see Fig. 3). In the first stage (*chromosome mask*), the segmentation of the DAPI channel takes place using Otsu's threshold selection method. Using the binary image produced in the previous stage, we extract all the pixels that belong to chromosomes. The *region segmentation* stage decomposes the M-FISH image into regions using the WT: the gradient magnitude of the multispectral image is computed. The goal of the next stage (*region characterization*) is the classification of each region of the M-FISH image. In order to achieve this, we first estimate the parameters of single-channel GMMs. Each single-channel GMM is used to describe the probability density of chromosome pixels from each channel of the M-FISH image. From this GMM, we estimate the parameters (mean, covariance, and mixture coefficient) of each chromosome class for a multichannel GMM. Finally, we make use of the MAP-EM algorithm in order to adapt the parameters of the multichannel GMM for each M-FISH image. Having computed the class parameters, all chromosome regions are classified into 1–24 chromosome classes. The final stage (*region merging*) is used to merge the classified regions producing a final classification map for the cytogeneticist.

A. Chromosome Mask

The first step of our method is the segmentation of the DAPI channel of the M-FISH image. This was realized using a non-parametric threshold selection technique. Otsu's method [24] computes automatically an optimal threshold value l^* that is found by maximizing the between class variance.

The binary image created by the Otsu method is defined as follows:

$$B_{Otsu}(i, j) = \begin{cases} 0, & \text{if } DAPI(i, j) \leq l^* \\ 1, & \text{if } DAPI(i, j) > l^* \end{cases}. \quad (1)$$

An example of the segmentation of the DAPI channel of an M-FISH image is shown in Fig. 4.

As a result of this task, the image pixels are classified as foreground pixels (called chromosome pixels) or background pixels. Suppose that, the segmented image B_{Otsu} contains N chromosome pixels and let X be the set of these chromosome pixels $X = \{x_1, x_2, \dots, x_N\}$. Each chromosome pixel is associated with a 5-D vector $x_k, k = 1, \dots, N$ containing the corresponding intensities of each of the five M-FISH image channels $x_k = (x_k^1, x_k^2, x_k^3, x_k^4, x_k^5)^T$. The intensities of the chromosome

pixels are normalized using the standard method

$$y_k^j = \frac{x_k^j - \mu^j}{\sigma^j}, \quad k = 1, \dots, N, j = 1, \dots, 5 \quad (2)$$

where μ^j is the mean and standard deviation of the chromosome pixels of the channel j . Thus, the set $Y = \{y_1, y_2, \dots, y_N\}$ is obtained (where $y_k \in \mathbb{R}^5$, $k = 1, \dots, N$ containing the corresponding normalized intensities of each of the five M-FISH image channels).

B. Region Segmentation

The WT is a widely used image-segmentation algorithm that originated from the field of mathematical morphology. The image is considered as a topographical relief, where the height of each pixel is related to its gray level. Assuming that imaginary rain falls on the terrain, the watersheds are the lines separating the catchment basins [25], [26]. In order to be able to apply the WT in a multichannel image, one has first to define the gradient. In our approach, instead of separately computing the scalar gradient from each image channel, we compute the tensor gradient [20], [27], [28].

A common problem of the application of the WT to the gradient image is oversegmentation [20]. This is due to the fact that the WT defines a distinct region for each regional minimum of the gradient image. On the other hand, the grayscale reconstruction [23], [29] suppresses all minima whose depth are lower than or equal to a threshold. Thus, we apply this procedure [20], [30], [31] in order to alleviate the over segmentation problem. The output of the WT for an image I is a tessellation T_I of the image into its different regions R_i , $1 \leq i \leq \text{NR}_i$ each one characterized by a unique label l_i .

$$T_I = \{(R_1, l_1), (R_2, l_2), \dots, (R_{\text{NR}_I}, l_{\text{NR}_I})\} \quad (3)$$

Thus, a new label image L_w is defined where each pixel is assigned a label. This label is the label of the region to which it belongs. All pixels corresponding to the watershed lines are assigned a special label, e.g., 0

$$L_W(i, j) = \begin{cases} l_k, & \text{if the pixel } (i, j) \in R_k \\ 0, & \text{if the pixel } (i, j) \in \text{Watershed Line} \end{cases} \quad (4)$$

From the tessellation of the M-FISH image, we create a new labeled image W_{Lines} :

$$W_{\text{Lines}}(i, j) = \begin{cases} 0, & \text{if } L_W(i, j) \in \text{Watershed Line} \\ 1, & \text{otherwise} \end{cases} \quad (5)$$

Finally, the watershed lines are used to segment the regions produced from the binary image B_{Otsu} .

$$B_{\text{Regions}} = B_{\text{Otsu}} \bullet W_{\text{Lines}} \quad (6)$$

where \bullet is the logical AND operator. At the end of this step, all connected components which are not "0" are labeled with a unique region label. An example of the computation of the watershed region tessellation step is shown in Fig. 5.

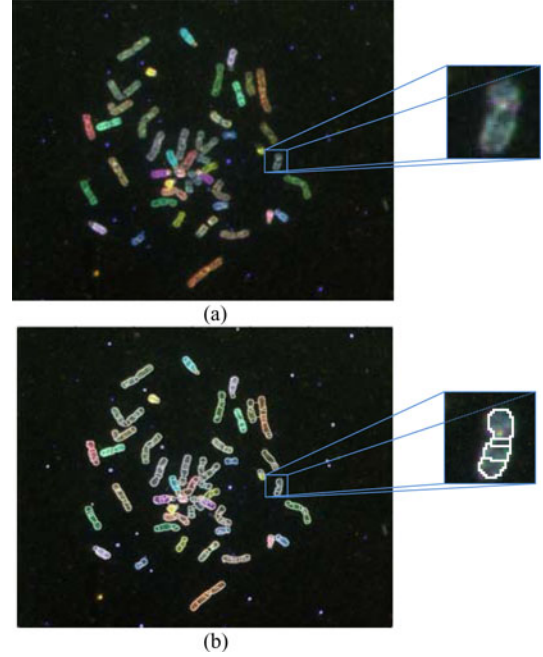


Fig. 5. Watershed segmentation of an M-FISH image. (a) The M-FISH image, (b) watershed regions superimposed on the M-FISH image.

C. Region Characterization

Each chromosome pixel $y \in \mathbb{R}^5$ is associated with a 5-D vector, containing the normalized intensities of each of the five M-FISH image channels. We wish to partition the chromosome pixels into $\sigma^j K = 24$ groups equal to the number of chromosome classes. This can be done by using any clustering algorithm. Our approach is based on the GMM in which one assumes that the pixels were sampled from multiple Gaussian components, such that each component corresponds to one chromosome class. The assignment of pixels to classes can then be easily performed by computing the posterior probability of a pixel to a class (see Section II-C3). Having described all that, the distribution of the chromosome pixels y could be modeled using a multidimensional GMM (called multichannel GMM) with K components, one for each chromosome class

$$p(y) = \sum_{i=1}^K \pi_i \cdot N(y; \mu_i, \Sigma_i) \quad (7)$$

where π_i is the mixing probability or the prior probability of the i th chromosome class, $N(y; \mu_i, \Sigma_i)$ is a Gaussian distribution with $\mu_i \in \mathbb{R}^5$ the mean and Σ_i the 5×5 covariance of the i th chromosome class, $i = 1, \dots, K$. A standard approach to learn the parameters of each chromosome class $(\pi_i, \mu_i, \Sigma_i, i = 1, \dots, K)$ is the EM algorithm. However, a common problem of the aforementioned approach (EM algorithm) is the initialization of the parameters of each chromosome class. This is due to the fact that the EM algorithm converges to a local maximum of the likelihood that highly depends on the initial parameter values. Next, we describe a novel process for the initialization of the multichannel GMM.

1) *Chromosome-Distribution Estimation*: At first, we compute initial values $(\tilde{\pi}_i, \tilde{\mu}_i, \tilde{\Sigma}_i, i = 1, \dots, K)$ for the parameters of each chromosome class. The initialization step is composed of following two procedures:

- 1) *Single-channel GMM estimation*: For each channel a two GMM is estimated: the first component corresponds to pixels belonging to hybridized chromosomes (brighter in the image) and the second component corresponds to pixels belonging to nonhybridized chromosomes (darker in the image).
- 2) *Multichannel GMM initialization*: Using the above single-channel GMMs, we compute an initialization of the 24-component multichannel GMM that models the distributions over the 5-D M-FISH image space.

a) *Single-channel GMM estimation*: Each channel j of the M-FISH image (except the DAPI channel) contains chromosome pixels that either belong to hybridized chromosome or to nonhybridized chromosomes. Thus, the distribution of the grayscale values y_k^j is modeled using a mixture of two Gaussians [21]

$$p(y_k^j) = p(y_k^j | C_h^j) P(C_h^j) + p(y_k^j | C_{nh}^j) P(C_{nh}^j) \quad (8)$$

where y_k^j is the intensity of a chromosome pixel k in channel j , $p(y_k^j | C_h^j)$ is the probability of pixel k to be hybridized in channel j , $p(y_k^j | C_{nh}^j)$ is the probability of pixel k to be nonhybridized in channel j , and C_h^j, C_{nh}^j are the hybridized and nonhybridized classes, respectively. Also, $p(y_k^j | C_h^j) \sim N(\mu_h^j, (\sigma_h^j)^2)$ and $p(y_k^j | C_{nh}^j) \sim N(\mu_{nh}^j, (\sigma_{nh}^j)^2)$, $X = \{x_1, x_2, \dots, x_N\}$, σ_h^j are the mean intensity and standard deviation of the hybridized pixels of channel j , respectively, whereas $\mu_{nh}^j, \sigma_{nh}^j$ are the mean intensity and standard deviation of the nonhybridized pixels of channel j , respectively. Finally, $P(C_h^j)$ and $P(C_{nh}^j)$ are the prior probabilities for the hybridized and nonhybridized classes, for channel j , respectively, that sum to 1.

For the estimation of the parameters $\{\{\mu_h^j, \sigma_h^j, \mu_{nh}^j, \sigma_{nh}^j, P(C_h^j), P(C_{nh}^j)\}, j = 1, \dots, 5\}$ of the GMMs, we employed the well-known EM algorithm [32]. The EM algorithm is an iterative algorithm which at each iteration consists of two steps, the expectation (*E-step*) and the maximization step (*M-step*).

E-step: Given the parameter estimates at iteration t , denoted as $\{\{\mu_h^{j(t)}, \sigma_h^{j(t)}, \mu_{nh}^{j(t)}, \sigma_{nh}^{j(t)}, P(C_h^{j(t)}), P(C_{nh}^{j(t)})\}, j = 1, \dots, 5\}$, we compute the posterior probabilities

$$P^{(t)}(C_h^j | y_k^j) = \frac{P^{(t)}(C_h^j) \cdot p^{(t)}(y_k^j | C_h^j)}{P^{(t)}(C_h^j) \cdot p^{(t)}(y_k^j | C_h^j) + P^{(t)}(C_{nh}^j) \cdot p^{(t)}(y_k^j | C_{nh}^j)} \quad (9)$$

$$P^{(t)}(C_{nh}^j | y_k^j) = \frac{P^{(t)}(C_{nh}^j) \cdot p^{(t)}(y_k^j | C_{nh}^j)}{P^{(t)}(C_h^j) \cdot p^{(t)}(y_k^j | C_h^j) + P^{(t)}(C_{nh}^j) \cdot p^{(t)}(y_k^j | C_{nh}^j)} \quad (10)$$

M-step: Update the parameters using

$$\Lambda_h = \sum_{k=1}^N P^{(t)}(C_h^j | y_k^j) \quad (11)$$

$$\Lambda_{nh} = \sum_{k=1}^N P^{(t)}(C_{nh}^j | y_k^j) \quad (12)$$

$$P^{(t+1)}(C_h^j) = \frac{\Lambda_h}{N} \quad (13)$$

$$P^{(t+1)}(C_{nh}^j) = \frac{\Lambda_{nh}}{N} \quad (14)$$

$$\mu_h^{j(t)} = \frac{\sum_{k=1}^N P^{(t)}(C_h^j | y_k^j) \cdot y_k^j}{\Lambda_h} \quad (15)$$

$$\mu_{nh}^{j(t)} = \frac{\sum_{k=1}^N P^{(t)}(C_{nh}^j | y_k^j) \cdot y_k^j}{\Lambda_{nh}} \quad (16)$$

$$\sigma_h^{j(t)} = \sqrt{\frac{1}{\Lambda_h} \sum_{k=1}^N P^{(t)}(C_h^j | y_k^j) \cdot (y_k^j - \mu_h^{j(t)})^2} \quad (17)$$

The EM algorithm is a local optimization algorithm, thus, it is sensitive to initial values of the parameters. In order to overcome this problem, we are going to exploit prior information about our problem. More specifically for the priors $P(C_h^j)$ and $P(C_{nh}^j)$, we exploit the emission information about the chromosome classes (see Appendix A). It is well known that the chromosome class index reflects the size of each chromosome in descending order (i.e., chromosome 1 is the largest and chromosome 22 is the smallest [20]). Thus, it is easy to estimate the proportion A_i of pixels belonging to chromosome class i either from a small set of M-FISH images [20] or to define it using medical knowledge [1]. Consequently, we can define the initial prior $P^{(t=0)}(C_h^j)$ as the proportion of the pixels that belong to the hybridized pixels for channel j as follows:

$$P^{(t=0)}(C_h^j) = \frac{\sum_{i=1}^K \Phi_{ij} A_i}{\sum_{i=1}^K A_i} \quad (18)$$

where the matrix Φ is defined as (see Appendix A) follows:

$$\Phi_{ij} = \begin{cases} 1, & \text{if chromosome class } i \text{ emits on channel } j \\ 0, & \text{otherwise} \end{cases} \quad (19)$$

and $P^{(t=0)}(C_{nh}^j) = 1 - P^{(t=0)}(C_h^j)$.

Since the data have been normalized (2) the initial values for mean and standard deviations for the components of nonhybridized pixels are set to -1 and 1 , respectively, and the mean and standard deviations for the components of the hybridized pixels are set to 1 .

$$\mu_h^{j(t=0)} = 1, \sigma_h^{j(t=0)} = 1 \quad (20)$$

$$\mu_{nh}^{j(t=0)} = -1, \sigma_{nh}^{j(t=0)} = 1 \quad (21)$$

b) *Multichannel GMM estimation*: The goal of this step is to compute an initial estimation of the chromosome class parameters $(\tilde{\pi}_i, \tilde{\mu}_i, \tilde{\Sigma}_i, i = 1, \dots, K)$ of the multichannel GMM

using the emission information that we are going to exploit for each chromosome class.

First, we have to take into consideration some key points about the emission information of each chromosome class. If a chromosome of class C_i emits in channel j , then the probability of a pixel k belonging to that chromosome would be equal to the probability $p(y_k^j|C_i^j)$ of that pixel to be hybridized in this channel. Vice versa, if a chromosome of class C_i does not emit in channel j , then the probability of a pixel which has been computed from the single-channel GMM belonging to that chromosome would be equal to the probability of that pixel to be nonhybridized $p(y_k^j|C_{nh}^j)$ in channel j . Based on the previous fact, we can define the probability $\tilde{p}(y_k^j|C_i)$ of a chromosome pixel y_k^j in channel j belonging to chromosome class C_i using the emission matrix Φ as follows:

$$\tilde{p}(y_k^j|C_i) = \Phi_{ij}p(y_k^j|C_h^j) + (1 - \Phi_{ij})p(y_k^j|C_{nh}^j) \quad (22)$$

where C_i are the 24-chromosome classes and $1 \leq j \leq 5$.

For example, the probability that a chromosome pixel of channel $j = 4$ belonging to chromosome C_1 is as follows:

$$\tilde{p}(y_k^4|C_1) = \Phi_{14}p(y_k^4|C_h^4) + (1 - \Phi_{14})p(y_k^4|C_{nh}^4). \quad (23)$$

Using the emission matrix Φ (from Appendix A, we can see that chromosome 1 emits in channel 4, thus, $\Phi_{14} = 1$) and substituting in following equation, we get

$$\tilde{p}(y_k^4|C_1) = p(y_k^4|C_1) \quad (24)$$

Using this assumption, we are going to derive our initial estimation for the prior, mean and covariance parameters of each class distribution $(\tilde{\pi}_i, \tilde{\mu}_i, \tilde{\Sigma}_i, i = 1, \dots, K)$. The initial mean of each chromosome distribution, $1 \leq i \leq K$ is computed by estimating each $\tilde{\mu}_i^j, 1 \leq j \leq 5$ using (23) as follows:

$$\tilde{\mu}_i^j = \Phi_{ij}\mu_h^j + (1 - \Phi_{ij})\mu_{nh}^j, \quad j = 1, \dots, 5. \quad (25)$$

Furthermore, the initial covariance $\tilde{\Sigma}_i$ of each chromosome's distribution, $1 \leq i \leq K$, is computed using (23) as follows:

$$\tilde{\Sigma}_i = \text{diag}((\sigma_i^1)^2, (\sigma_i^2)^2, (\sigma_i^3)^2, (\sigma_i^4)^2, (\sigma_i^5)^2) \quad (26)$$

where $(\sigma_i^j)^2 = (\Phi_{ij})^2(\sigma_h^j)^2 + (1 - \Phi_{ij})^2(\sigma_{nh}^j)^2, j = 1, \dots, 5$.

Finally, the prior probability is the expected proportion of pixels belonging to a specific chromosome [20]

$$\tilde{\pi}_i = A_i, \quad i = 1, \dots, K. \quad (27)$$

2) *Chromosome-Distribution Estimation*: Having estimated the initial parameters for the multichannel GMM, our goal is to allow the parameters to be further adapted. Instead of estimating the GMM parameters via the EM algorithm, we employ maximum a posteriori (MAP) for parameter estimation, since we already have incorporated prior knowledge (such as the emission information) to our initial model. More specifically, we have used the MAP-EM algorithm [33] which exploits prior information. Like the EM algorithm, the MAP estimation is a two-step estimation process. The first step is identical to the ‘‘Expectation’’ step of the EM algorithm. Unlike the M -step of the EM algorithm, in the M -step of MAP-EM, parameters are obtained by taking into account the initial model.

The parameters $\{\pi_1^{(t)}, \mu_1^{(t)}, \Sigma_1^{(t)}, \dots, \pi_K^{(t)}, \mu_K^{(t)}, \Sigma_K^{(t)}\}$ are initialized using the values from the previous step e.g.,

$$\left. \begin{aligned} \pi_i^{(t=0)} &= \tilde{\pi}_i \\ \mu_i^{(t=0)} &= \tilde{\mu}_i \\ \Sigma_i^{(t=0)} &= \tilde{\Sigma}_i \end{aligned} \right\}, 1 \leq i \leq K. \quad (28)$$

The MAP-EM estimation of the GMM parameters is described as follows [33]:

E-step: In the E -step similarly to the previous case, given the estimation of parameters at iteration $t \{\pi_1^{(t)}, \mu_1^{(t)}, \Sigma_1^{(t)}, \dots, \pi_K^{(t)}, \mu_K^{(t)}, \Sigma_K^{(t)}\}$, we calculate

$$v_i^{(t)}(y_k) = \frac{\sum_{k=1}^N p(y_k|C_i)}{\sum_{j=1}^K \sum_{k=1}^N p(y_k|C_j)} \quad (29)$$

$$E_i^{(t)}(y_k) = \frac{\sum_{k=1}^N y_k p(y_k|C_i)}{\sum_{k=1}^N p(y_k|C_i)} \quad (30)$$

$$E_i^{(t)}(y_k y_k^T) = \frac{\sum_{k=1}^N y_k y_k^T p(y_k|C_i)}{\sum_{k=1}^N p(y_k|C_i)} \quad (31)$$

M-step: The M -step is described by the following update equations:

$$\pi_i^{(t+1)} = (1 - a)v_i^{(t)}(y_k) + \alpha\tilde{\pi}_i \quad (32)$$

$$\mu_i^{(t+1)} = (1 - \beta)E_i^{(t)}(y_k) + \beta\tilde{\mu}_i \quad (33)$$

$$\begin{aligned} \Sigma_i^{(t+1)} &= (1 - \gamma)E_i^{(t)}(y_k y_k^T) + \gamma \left[\tilde{\Sigma}_i + \tilde{\mu}_i \tilde{\mu}_i^T \right] \\ &\quad - \mu_i^{(t+1)} \left[\mu_i^{(t+1)} \right]^T \end{aligned} \quad (34)$$

where the parameters a, β , and γ are the learning rates, which define how confident we are about the prior values $\tilde{\pi}_i, \tilde{\mu}_i, \tilde{\Sigma}_i, i = 1, \dots, K$.

Note that in the M -step, the updates of the parameters (33)–(35) are made using a combination of the updates suggested by the typical EM (first term of the sum) and the initial model we have computed in the initialization phase (see Section II-C1).

3) *Region Classification*: Having estimated the parameters $(\pi_i, \mu_i, \Sigma_i, 1 \leq i \leq K)$ of each chromosome class, we could classify a pixel $y \in \mathbb{R}^5$ to a chromosome class $C_i, 1 \leq i \leq K$ using the posterior probability $P(C_i|y)$:

$$P(C_i|y) = \frac{p(y|C_i)P(C_i)}{\sum_{i=1}^K p(y|C_i)P(C_i)}. \quad (35)$$

The class, to which the pixel is assigned, is given by the Bayes decision rule [34]

$$\text{decide } C_i \text{ if } P(C_i|y) > P(C_j|y) \quad \forall j \neq i, i = 1, \dots, K \quad (36)$$

However, our goal is to take advantage of the region segmentation stage and to classify each whole region of our M-FISH image. Suppose a regions $R_p, 1 \leq p \leq NR_I$, that consists of NP pixels $\{y_1, y_2, \dots, y_{NP}\}$, where $y_i \in \mathbb{R}^5, i = 1, \dots, NP$ denotes a 5-D vector containing the 5-normalized intensities of a pixel of each channel. We then compute the average posterior probability for each one of the 24-chromosome classes as

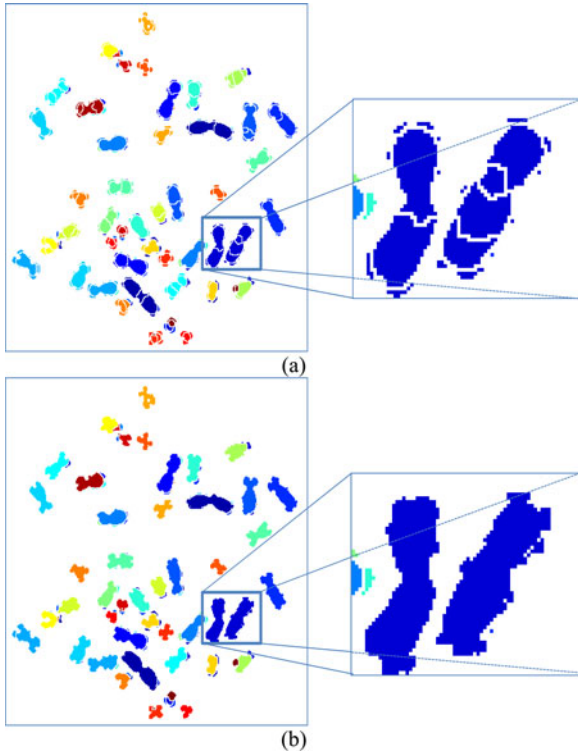


Fig. 6. Region merging of chromosomes. (a) Initial classification map (we have used a separate color for each chromosome class), (b) merging of adjacent regions of the same class.

follows:

$$P_{\text{Avg}}(C_i|R_p) = \frac{1}{\text{NP}} \sum_{l=1}^{\text{NP}} P(C_i|y_l) \quad (37)$$

Finally, we classify the region R_p , $1 \leq p \leq NR_I$ to the chromosome class j that has the highest average posterior probability

$$P_{\text{Avg}}(C_j|R_p) > P_{\text{Avg}}(C_i|R_p), \forall i \neq j, 1 \leq i \leq K \quad (38)$$

D. Region Merging

The next step of our method is region merging. Note that there are still regions that could be merged resulting into a meaningful classification map. First, adjacent regions that share the same class are merged into one single region. In order to connect the adjacent regions, the region adjacency graph (RAG) is computed for the image [35]. The RAG is a graph where two nodes (representing two regions) are connected if those two regions are adjacent in the image. Thus, each region of the image is connected to all regions that share the same class. An example is shown in Fig. 6(a) and (b).

We must mention how our algorithm deals with cases of touching chromosomes/overlaps. In the case of touching chromosomes

- 1) If the chromosomes are classified into two different classes, then the chromosomes are not merged.
- 2) If the chromosomes are classified into the same class, then our method will merge them.

In our database, we excluded areas of overlaps since there is no information in the database which chromosomes classes are present in the overlap area.

It has been observed that small regions are often misclassified by our region classification step. In order to tackle this problem, we have adopted the following procedure. First, all small regions are identified. We define a small region as the region whose number of pixels is lower than a threshold. This threshold must be lower than the number of pixels of the smallest chromosome of the database and must be adapted for each M-FISH image M_i , $i = 1, \dots, F$ of our database (where F is the total number of images of the M-FISH database). We define P_i the number of chromosome pixels of the i th M-FISH image. Let us assume that the M-FISH image with the smallest chromosome is M_s and SCP the number of pixels of this chromosome. Thus, the proportion of pixels for the smallest chromosome for this image will be as follows:

$$T_s = \frac{\text{SCP}}{P_s} \quad (39)$$

where P_s is the number of chromosome pixels of the image containing the smallest chromosome and T_s is the proportion of the pixels for the smallest chromosome of this image.

Finally, we compute the pixel threshold T_i for each M-FISH image M_i , $i = 1, \dots, F$ of our database as follows:

$$T_i = T_s \cdot P_i. \quad (40)$$

Assume now a small region R of an M-FISH image where the #pixels of region $R \leq T_i$. We can use the RAG to select the neighbors of R : $N_R = \{R_1, R_2, \dots, R_G\}$. Let C_i the class of region $R_i \in N_R$, $i = 1, \dots, G$ and $Q = \{C_1, C_2, \dots, C_G\}$ the set of these classes. Then, we compute the posterior probabilities $P_{\text{Avg}}(C_i|R)$ for each $C_i \in Q$ and select the class C_j with maximum posterior

$$P_{\text{Avg}}(C_j|R) \geq P_{\text{Avg}}(C_i|R), \forall C_i \in Q. \quad (41)$$

Then region R is merged with a region R_j whose class is C_j . An example of the application of this step is shown in Fig. 7(a) and (b).

III. RESULTS

A. Dataset

In order to test our method, we have used the Advanced Digital Imaging Research (ADIR) M-FISH database [16]. This database consists of M-FISH images that were produced using probe sets from applied spectral imaging, PSI (former ADIR), and Vysis—the three probes that were used for the specimens (see Appendix A). Table I, describes the number of images for each set [21]. Each M-FISH consists of different channels and a DAPI channel. The quality of the spread ranges from excellent to very low. Finally, an annotated image is provided with each M-FISH image set. This image is labeled so that the gray level of each pixel represents its class number (chromosome class). In addition, background pixels are labeled as 0, and pixels in a region of overlap are labeled as -1 .

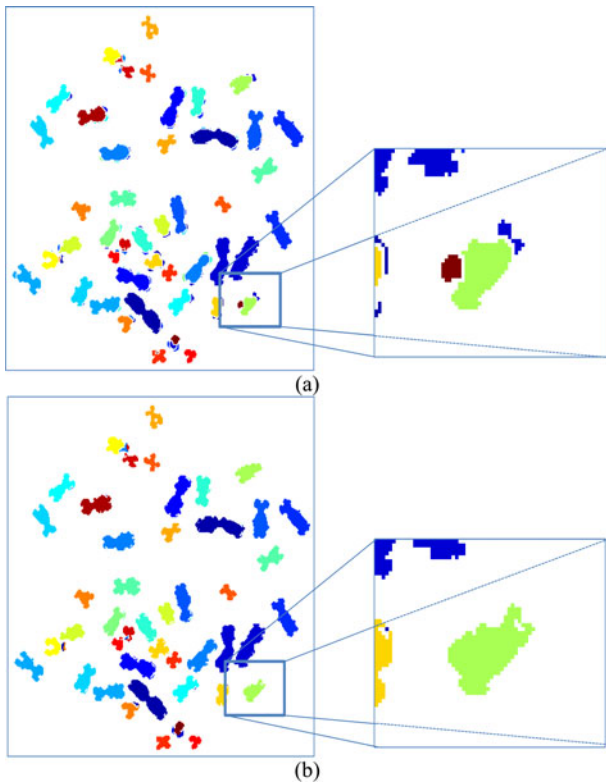


Fig. 7. Region merging of chromosomes. (a) Initial classification map (we have used a separate color for each chromosome class), (b) merging of adjacent regions of the same class.

TABLE I
NUMBER OF IMAGES FOR EACH SET

Probe Set	#Images
Applied Spectral Imaging	85
PSI	71
Vysis	29

There are many images that give low-classification accuracy [21], where the classification accuracy is defined as follows:

$$\text{Accuracy} = \frac{\# \text{ of correctly chromosome pixels}}{\text{total} \# \text{ of chromosome pixels}}. \quad (42)$$

The common factor among those images is that the image quality is poor. These images were self-trained and tested using a Bayes pixel-by-pixel classifier [11], [16], [20], [21]. Those images that gave lower classification accuracy than 85% were identified (also visually confirmed) as bad images [21] (a list of the images is provided by Choi *et al.* [21]).

B. Parameter Estimation

In order to estimate the learning rates α, β , and γ , we conducted the following experiment. We varied the values of the learning rates as follows $\alpha = [0, 0.05, 0.1, \dots, 1]$, $\beta = [0, 0.05, 0.1, \dots, 1]$, and $\gamma = [0, 0.05, 0.1, \dots, 1]$ and computed the classification accuracy for these values. We then selected the values of the parameters having the highest classification accuracy. The best accuracy was observed for learning rates equal

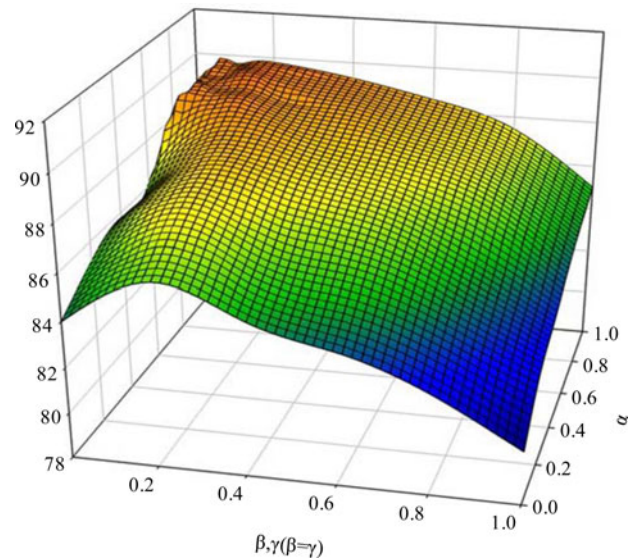


Fig. 8. Classification accuracy for several values of the learning rates α, β , and γ .

to $\alpha = 0.9, \beta = \gamma = 0.2$. Fig. 8 presents the accuracy of our method using these values for the ADIR M-FISH database.

The values of the parameters alpha, beta, and gamma control the certainty of how confident we are of the initial model ($\tilde{\pi}_i, \tilde{\mu}_i, \tilde{\Sigma}_i, i = 1, \dots, K$). This is described by (32)–(34). Values around zero would mean that we are not very certain of our initial model and values around one means that we are confident of the initial model. Thus, the parameter values $\alpha = 0.9$ means that we are 90% confident for the $\tilde{\pi}_i, i = 1, \dots, K$ values and $\beta = \gamma = 0.2$ means that we are 20% confident for the $\tilde{\mu}_i, \tilde{\Sigma}_i, i = 1, \dots, K$.

C. Classification Accuracy

The best overall classification accuracy for all the M-FISH images was found to be 89.95%. The learning rates are computed for the ADIR M-FISH image dataset. However, this database contains three different M-FISH datasets produced by three different kits. Thus, the estimation is not required for a new kit. However, note that when the learning rates are set to $\alpha = \beta = \gamma = 0.0$, thus, the MAP-EM algorithm degenerates to the classical EM estimation, the classification accuracy reduces to 83.62%. This proves the effectiveness of the MAP-EM algorithm over the classical EM algorithm. Fig. 9 presents the class classification accuracy for the best parameters values mentioned previously.

D. Translocation Detection and Limitations

Translocation is the most significant rearrangement. It involves two nonhomologous chromosomes which result from a break in each of the chromosomes, and subsequent reunion [36]. A change in the color of a chromosome tip may be due to noise, staining, or an actual translocation. Fig. 10, (Case A), presents a translocation between chromosome classes 9 and 4. As it can be

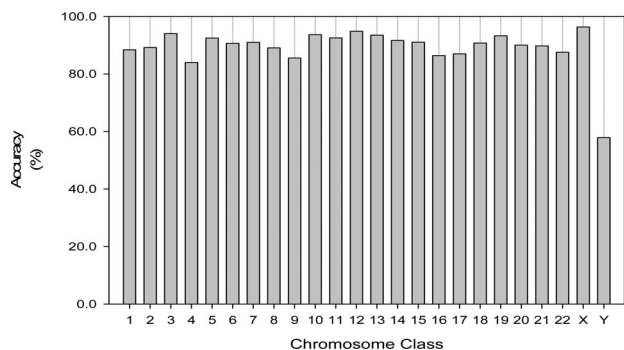


Fig. 9. Classification accuracy for each of the chromosome classes (1, 2, ..., 22, X, Y).

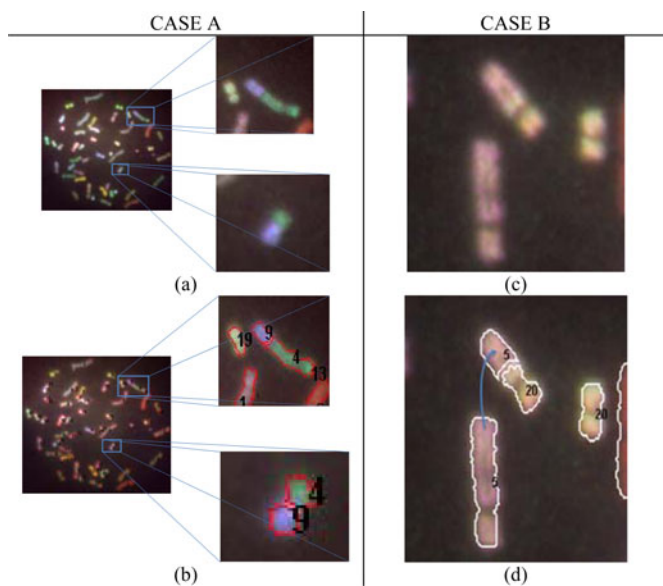


Fig. 10. Two examples of accurate detection and classification of exchange of genetic material. CASE A: Translocation between two different chromosomes (green chromosome 4 and blue chromosome 9). (a) Two translocated chromosomes. (b) Translocation detected by our method. A fragment of chromosome 9 has been inserted into chromosome 4. Vice versa, a fragment of chromosome 4 has been inserted into chromosome 9. CASE B: Insertion between two different chromosomes (chromosome 5 and chromosome 20). (c) Chromosomes. (d) Fragment of chromosome 5 has been inserted into chromosome 20.

observed for this example, our method segments and classifies correctly the translocated fragments.

Insertion is the chromosome abnormality where a fragment of a chromosome is inserted to another chromosome. However, since our method can detect translocations where fragments of two chromosomes are exchanged, the insertion abnormality will also be detected by our method. Fig. 10, (Case B), displays an example of correct segmentation and classification of an insertion abnormality.

However, our method presents some limitations that need discussion. One of the limitations was the misclassifications of small regions. These regions had the number of pixels smaller than the threshold computed by (40). In order to classify them correctly, we select these regions (39) and reclassified them to the neighbor, maximizing the posterior probability of this neigh-

bor. This procedure helped our method to classify correct those regions. However, if a fragment of a chromosome belonging to a translocation is smaller than the smallest chromosome this will be probably merged to the neighbor chromosome. This is a drawback of our method. However, as we have described previously, there is a tradeoff between reducing misclassifications and detecting translocations.

Another limitation of our method has been already described by our segmentation procedure [20]. If a segmentation error occurs then this type of error could not be corrected by the classification procedure. A possible solution to this would be the two procedures to be combined together. For example, each region that is defined by the segmentation procedure could be verified by the classification procedure. Also, if two chromosomes of the same class are adjacent then our merging procedure would erroneously merge them.

IV. DISCUSSION AND CONCLUSION

We described a novel fully unsupervised method for the classification of M-FISH images. The method first uses a watershed based algorithm to segment the M-FISH image into regions. Next, our goal is to partition the chromosome pixels by a GMM with $K = 24$ components, one for each chromosome class. However, following two main problems had to be overcome.

- 1) *The initialization of the multichannel GMM:* We first estimate five, two-component single-channel GMMs where the first component corresponds to the hybridized class and the second to the nonhybridized class. We then combine those GMMs in order to estimate an initial multichannel GMM. Furthermore, we incorporate to this model the emission information that we had from the M-FISH experiment (presented in Appendix A).
- 2) *The adaptation of the parameters of the multichannel GMM:* Although we could adapt this multichannel Gaussian model using the EM algorithm, we chose to employ the MAP-EM method which uses the initial model build in the previous step. This proves to be more efficient in terms of classification accuracy from the classical application of the EM algorithm. More specifically the MAP-EM method (89.95%) attains an increase 6.33%, over the application of the classical EM (83.62%).

Having estimated the multichannel GMM, we then classify each region of the M-FISH image. Finally, a region merging step is utilized in order to produce a final classification map to the cytogeneticist.

Several methods have been proposed in the literature for the M-FISH chromosome image classification. Most of these methods are supervised requiring a small number of images to train the classifier. Supervised classification methods, such as the Bayes classifier and k-nearest neighbor require training data [14]. However, collecting and labeling a large set of samples can be extremely costly. Additionally significant variations have been observed between the M-FISH images. These variations are often due to a lot of factors such as long exposure times, humidity, temperature, type of microscope, and color spread [21]. When a supervised classification method is used, the

TABLE II
COMPARISON OF THE PROPOSED METHOD AND OTHER METHODS REPORTED IN
THE LITERATURE IN TERMS OF CHROMOSOME CLASSIFICATION ACCURACY

Method	Type of Classification		Database Used*	Average Chromosome Pixel Classification Accuracy (%)
Sampat et al. [11]	Pixel-by-Pixel	Supervised	A	91.4
Choi et al. [13]	Pixel-by-Pixel	Supervised	A	97.1
Sampat et al. [14]	Pixel-by-Pixel	Supervised	A	90.5
Wang et al. [15]	Pixel-by-Pixel	Supervised	A	87.5
Schwartzkopf et al. [16]	Pixel-by-Pixel	Supervised	C	68.0
Karvelis et al. [17]	Region Based	Supervised	A	89.0
Karvelis et al. [18]	Region Based	Supervised	C	82.5
Choi et al. [21]		Unsupervised	B	77.8
This method	Region Based	Unsupervised	B	89.95
	Region Based	Unsupervised	C	83.62
K-means [38]	Pixel-by-Pixel	Unsupervised	B	72.48

* A: Part of the database.

B: The whole ADIR database minus the Bad Images.

C: The whole ADIR database.

classification accuracy will be high when the sample distributions of both training and testing data are the same. However, this is often not the case making the need for a fully unsupervised M-FISH image classification method a necessity. Our method requires only the knowledge of the emission matrices (Appendix A) which is available upon the purchase of the kit; thus, making the M-FISH technique attractive for use when ground truth does not exist.

Table II, presents a comparison of several different classification algorithms presented in the literature. Most of the methods employ pixel-by-pixel classification schemes and use the whole or part of the ADIR M-FISH dataset. Supervised based methods were the first methods [11] that have been introduced for the classification of M-FISH images. The classification accuracy for the whole ADIR M-FISH database is 82.5%. However, the classification accuracy when we tested our method without the bad images [21], is 89.95%. Unsupervised based methods already have been tested for the whole database and their reported accuracy is 77.8% [21]. We have also tested the *K*-means algorithm for the ADIR M-FISH database, where we have used the emission information for each chromosome class in order

to initialize the cluster centers [37]. The classification accuracy was 72.48%. Our method is superior to both unsupervised and supervised methods as shown in Table II.

Fluorescent *in situ* hybridization (FISH) technology has been widely recognized as a promising molecular and biomedical optical imaging tool to screen and diagnose different types of chromosome anomalies that could be evolved in different types of cancer (e.g., trisomy of chromosomes 3, 7, X has a significant impact on cervical cancer development and prognosis [38]). One of the advantages of our method could be the application using different types of multichannel FISH images in order to correctly segment and classify not only chromosomes but also chromosome spots in general [38]. Furthermore, our method is independent of the number of channels used by the FISH technology (e.g., a two-image channel image is used by Wang et al. [38] to detect cervical cancer). The proposed approach could be employed to other color images that use the FISH technology. However, the matrices for the emission of each class like those described in the appendixes should be provided. Finally, the average time for the segmentation/classification stage is 55.4 s (± 8.5) using an Intel Core 2 Duo Processor PC, with 1 GB of RAM. Specifically, the average classification time was 27.3 s (± 8.1).

Summarizing, in this paper, we have proposed a new fully unsupervised automated approach for the segmentation and classification of M-FISH images. First, we segment the multichannel M-FISH image making use of the WT in order to segment the image into regions. This has the advantage that we classify regions that share the same spectral information and thus, acquire better classification results. However, the main novelty of this paper is the proposed GMM-based methodology for region classification. We propose an initialization of the GMM using the emission information of each chromosome class used in the M-FISH experiment. Then, we adapt this initial model using MAP estimation. As our experiments demonstrated, the use of this MAP approach acquires better classification results when compared with the classical EM algorithm. Finally, our method does not require any ground truth images and its classification accuracy is higher even when compared with supervised methods. We have not tested our methodology to other type of unsupervised imaging classification problems. This is due to the fact that the emission information for each class must be provided.

However, as for future work we intend to test our method to image analysis problems that use the FISH technology. Detection of chromosome abnormalities such as translocations is the final stage of a method for automated chromosome classification. However, one must first deal with the classification procedure and then focus on detecting chromosome abnormalities. This is the reason why we focused on developing an unsupervised method for M-FISH chromosome classification minimizing the misclassification rate.

APPENDIX

M-FISH emission charts for each chromosome class. Three different kits were used to produce the ADIR M-FISH database [16].

REFERENCES

- [1] M. Thompson, R. McInnes, and H. Willard, *Genetics Medicine*, 5th ed. Philadelphia, PA, USA: Saunders, 1991.
- [2] S. Heim and F. Mitelman, *Cancer Cytogenetics*, 3rd ed. New York, NY, USA: Wiley-Blackwell, 2009.
- [3] S. Uhrig, S. Schuffenhauer, C. Fauth, A. Wirtz, C. Daumer-Haas, C. Apacik, M. Cohen, J. Müller-Navia, T. Cremer, J. Murken, and M. Speicher, "Multiplex-FISH for pre- and postnatal diagnostic applications," *Amer. J. Hum. Genet.*, vol. 65, pp. 448–462, 1999.
- [4] R. Speicher, S. G. Ballard, and D. C. Ward, "Karyotyping human chromosomes by combinatorial multi-fluor FISH," *Nat. Genet.*, vol. 12, pp. 368–375, 1996.
- [5] E. Schrock, S. du Manoir, T. Veldman, B. Schoell, J. Wienberg, M. A. Ferguson-Smith, Y. Ning, D. H. Ledbetter, I. Bar-Am, D. Soenksen, Y. Garini, and T. Ried, "Multicolor spectral karyotyping of human chromosomes," *Science*, vol. 273, pp. 494–497, 1996.
- [6] R. Eils, S. Uhrig, K. Saracoglu, K. Satzler, A. Bolzer, I. Petersen, J. Chassery, M. Ganser, and M. R. Speicher, "An optimized fully automated system for fast and accurate identification of chromosomal rearrangements by multiplex-FISH (M-FISH)," *Cytogenet. Cell Genet.*, vol. 82, no. 3–4, pp. 160–171, 1998.
- [7] T. Liehr and U. Claussen, "Multicolor-FISH approaches for the characterization of human chromosomes in clinical genetics and tumor cytogenetics," *Current Genomics*, vol. 3, pp. 213–235, 2002.
- [8] T. Veldman, C. Vignon, E. Schröck, J. Rowley, and T. Ried, "Hidden chromosome abnormalities in haematological malignancies detected by multicolor spectral karyotyping," *Nat. Genet.*, vol. 15, pp. 406–410, Apr. 1997.
- [9] R. Eils, S. Uhrig, K. Saracoglu, K. Satzler, A. Bolzer, I. Petersen, J. Chassery, M. Ganser, and M. R. Speicher, "An optimized fully automated system for fast and accurate identification of chromosomal rearrangements by multiplex-FISH (M-FISH)," *Cytogenet. Cell Genet.*, vol. 82, no. 3–4, pp. 160–171, 1998.
- [10] K. Saracoglu, J. Brown, L. Kearney, S. Uhrig, J. Azofeifa, C. Fauth, M. Speicher, and R. Eils, "New concepts to improve resolution and sensitivity of molecular cytogenetic diagnostics by multicolor fluorescence in situ hybridization," *Cytometry*, vol. 44, no. 1, pp. 7–15, 2001.
- [11] M. P. Sampat, A. C. Bovik, J. K. Aggarwal, and K. R. Castleman, "Pixel-by-pixel classification of MFISH images," in *Proc. 24th IEEE Ann. Intern. Conf. Eng. Med. Biol. Soc.*, Houston, TX, USA, 2002, pp. 999–1000.
- [12] Y. Wang and A. Dandpat, "Classification of M-FISH images using fuzzy C-means clustering algorithm and normalization approaches," in *Proc. 38th IEEE Asilomar Conf. Signals, Syst. Comput.*, Pacific Grove, CA, USA, 2004, vol. 1, pp. 41–44.
- [13] H. Choi, K. R. Castleman, and A. Bovik, "Joint segmentation and classification of M-FISH chromosome images," in *Proc. 26th IEEE Ann. Intern. Conf. Eng. Med. Biol. Soc.*, San Francisco, CA, USA, 2004, pp. 1636–1639.
- [14] M. P. Sampat, A. C. Bovik, J. K. Aggarwal, and K. R. Castleman, "Supervised parametric and non-parametric classification of chromosome images," *Pattern Recognit.*, vol. 38, pp. 1209–1223, 2005.
- [15] Y. Wang and K. R. Castleman, "Normalization of multicolor fluorescence in situ hybridization (M-FISH) images for improving color karyotyping," *Cytometry*, vol. 64, pp. 101–109, 2005.
- [16] W. C. Schwartzkopf, A. C. Bovik, and B. L. Evans, "Maximum-likelihood techniques for joint segmentation-classification of multispectral chromosome images," *IEEE Trans. Med. Imag.*, vol. 24, pp. 1593–1610, Dec. 2005.
- [17] P. Karvelis, D. I. Fotiadis, M. Syrrou, and I. Georgiou, "A watershed based segmentation method for multispectral chromosome images classification," in *Proc. 28th IEEE Ann. Intern. Conf. Eng. Med. Biol. Soc.*, New York, NY, USA, 2006, pp. 3009–3012.
- [18] Y. Wang and A. Dandpat, "A hybrid approach of using wavelets and fuzzy clustering for classifying multispectral fluorescence in situ hybridization images," *Intern. J. Biom. Imag.*, vol. 2006, pp. 1–11, 2006.
- [19] H. Choi, K. R. Castleman, and A. C. Bovik, "Segmentation and fuzzy-logic classification of M-FISH chromosome images," in *Proc. IEEE Intern. Conf. Image Process.*, Atlanta, GA, USA, 2006, pp. 69–72.
- [20] P. Karvelis, A. Tzallas, D. I. Fotiadis, and I. Georgiou, "A multichannel watershed-based segmentation method for multispectral chromosome classification," *IEEE Trans. Med. Imag.*, vol. 27, no. 5, pp. 697–708, May 2008.
- [21] H. Choi, A. C. Bovik, and K. R. Castleman, "Feature normalization via expectation maximization and unsupervised nonparametric classification for M-FISH chromosome images," *IEEE Trans. Med. Imag.*, vol. 27, no. 8, pp. 1107–1119, Aug. 2008.
- [22] H. Choi, K. R. Castleman, and A. C. Bovik, "Color compensation of multicolor FISH images," *IEEE Trans. Med. Imag.*, vol. 28, no. 1, pp. 129–136, Jan. 2009.
- [23] L. Vincent, "Morphological grayscale reconstruction in image analysis: Applications and efficient algorithms," *IEEE Trans. Image Process.*, vol. 2, no. 2, pp. 176–201, Apr. 1993.
- [24] N. Otsu, "A threshold selection method from gray-level histograms," *IEEE Trans. Syst. Man, Cybern.*, vol. 9, no. 1, pp. 62–66, Jan. 1979.
- [25] L. Vincent and P. Soille, "Watershed in digital spaces: An efficient algorithm based on immersion simulations," *IEEE Trans. Pattern Anal. Mach. Intell.*, vol. 13, no. 6, pp. 583–598, Jun. 1991.
- [26] R. Gonzalez and R. Woods, *Digital Image Processing*, 2nd ed. Upper Saddle River, NJ, USA: Prentice-Hall, 2002.
- [27] A. Cumani, P. Grattoni, and A. Giuducci, "An edge-based description of color images," *Comput. Vis. Graph. Image Process.*, vol. 53, pp. 313–323, 1991.
- [28] C. Drewniok, "Multi-spectral edge detection—Some experiments on data from Landsat-TM," *Int. J. Remote. Sens.*, vol. 15, no. 18, pp. 3743–3765, 1994.
- [29] K. R. Castleman, *Digital Image Processing*. Upper Saddle River, NJ, USA: Prentice-Hall, 1996.
- [30] A. Fleming, S. Philip, K. Goatman, J. Olson, and P. Sharp, "Automated microaneurysm detection using local contrast normalization and local vessel detection," *IEEE Trans. Med. Imag.*, vol. 25, no. 9, pp. 1223–1232, 2006.
- [31] P. Soille, *Morphological Image Analysis: Principles and Applications*, 2nd ed. Berlin, Germany: Springer-Verlag, 2003.
- [32] A. Dempster, N. Laird, and D. Rubin, "Maximum likelihood from incomplete data via the EM algorithm," *J. Roy. Statist. Soc. B*, vol. 39, pp. 1–38, 1977.
- [33] D. Reynolds, T. Quatieri, and R. Dunn, "Speaker verification using adapted Gaussian mixture models," *Digital Signal Process.*, vol. 10, pp. 19–41, 2000.
- [34] K. Fukunaga, *Introduction to Statistical Pattern Recognition*. San Diego, CA, USA: Academic Press, 1990.
- [35] K. Haris, S. Efstratiadis, N. Maglaveras, and A. Katsaggelos, "Hybrid image segmentation using watersheds and fast region merging," *IEEE Trans. Image Process.*, vol. 7, no. 12, pp. 1684–1699, Dec. 1998.
- [36] I. Belyaev, "Molecular targets and mechanisms in formation of chromosomal aberrations: Contributions of soviet scientists," *Cytogenet. Genome Res.*, vol. 104, pp. 56–64, 2004.
- [37] P. Karvelis, A. Likas, and D. Fotiadis, "Semi Unsupervised M-FISH chromosome image classification," in *Proc. 10th IEEE Intern. Conf. Inf. Technol. Appl. Biomed.*, Corfu, Greece, 2010, pp. 1–4.
- [38] X. Wang, B. Zheng, S. Li, R. Zhang, J. Mulvihill, W. Chen, and H. Liu, "Automated detection and analysis of fluorescent in situ hybridization spots depicted in digital microscopic images of Pap-smear specimens," *J. Biomed. Opt.*, vol. 14, no. 2, pp. 1–8, 2009.



Petros S. Karvelis was born in Mesologi, Greece, in 1978. He received the Diploma, M.Sc., and Ph.D. degrees in computer science from the University of Ioannina, Ioannina, Greece, in 2001, 2004, and 2012, respectively.

His research interests include medical image processing, and biomedical engineering.



Aristidis C. Likas (SM'03) received the Diploma degree in electrical engineering and the Ph.D. degree in electrical and computer engineering from the National Technical University of Athens, Athens, Greece, in 1990 and 1994, respectively.

Since 1996, he has been with the Department of Computer Science, University of Ioannina, Ioannina, Greece, where he is currently an Associate Professor. His research interests include neural networks, machine learning, statistical signal processing, and bioinformatics.